Indian Journal of Science and Technology, Vol 11(48), DOI: 10.17485/ijst/2018/v11i48/138799, December 2018
ISSN (Print) : 0974-6846
ISSN (Online) : 0974-5645

Numerical Simulation of Ferromagnetic Fluid Flow in a Square Open Channel of Infinite Axial Length under the Effect of a Rotative Magnetic Field

Cristian Jimenez, Hermann Vargas and Rodrigo Correa*

Universidad Industrial de Santander, Bucaramanga, Santander, Colombia; cristian.jimenez@correo.uis.edu.co, hrvargas@uis.edu.co, crcorrea@saber.uis.edu.co

Abstract

Objectives: This article presents the results of simulations that describe the simultaneous effect of tangential stresses and volumetric stresses, in the generation of velocity profiles in a ferrofluid. **Methods:** The system of ferrohydrodynamic equations was solved by means of finite differences for both the dynamic and the magnetic problem, separately. For the present case, the flow was considered in a channel of square cross-section, under the effect of a rotating magnetic field of high magnitude and frequency. **Findings:** The results obtained show that the tangential stresses are more representative than the volumetric stresses in the flow generation. Likewise, it was observed that the lateral walls of the geometry generate counter-rotation in the translational velocity profiles, reaching saturation with the increasing of the magnetic field intensity, situation reported in the literature for experimental measurements. **Applications:** A complete understanding of this process will facilitate the design of new ferrofluid systems under the effect of rotating magnetic fields.

Keywords: Ferromagnetic Fluids, Rotative Magnetic Fields, Spin Theory, Spin Viscosity, Volumetric Stresses

1. Introduction

There is a great amount of physical phenomena induced by the presence of magnetic fields. Within this extensive area, it has been possible to classify specific topics such as magnetorheology, magnetohydrodynamics and ferrohydrodynamics, among others. The latter has received very little attention from researchers compared with, for example, magnetohydrodynamics, where SCOPUS (RM) reports for the first only 151 documents (1964-2019), while for the second 31917 (1952-2019). Despite this situation, there is a great potential to the application of ferrohydrodynamics, especially in areas such as medicine and fluid transport, as an example of this trend, recently[1]. Reported a study based on the fundamentals of ferrohydrodynamics, analyzing the effect on the heat transfer and blood flow in a channel of to the presence of a permanent magnetic field. They simulate this process by discretizing the model using the finite volume method, together with the material balance equation. Among its findings, it is highlighted that according to the simulations, there is an increase in the heat flow from the inside of the blood stream (in the presence of a magnetic drug) to the encloses. Likewise, they found that the loss of energy was due to the existence of shear stresses. Something additional that stands out is related to the occurrence of an increase in the transfer of heat from the inside of the blood flow (in the presence of a magnetic drug) to the walls, on the other hand, and in a recently reported work[2]. Numerically simulated the effect of a not uniform magnetic field on the flow of a biomagnetic fluid in a duct with an adjustable choke. They analyzed the influence of varying the strength of the magnetic field and the percentage of the opening of the strangulation on the flow

*Author for correspondence

of the magnetic material. Their results show an evident relationship between the magnetic field intensity and the flow of the biomagnetic material. It is important near the origin of the magnetic field (a wire that carries a variable current for this case and at a distance from the pipeline that carries the biomagnetic material). Applying a field of sufficient intensity, they found that downstream of the restriction considerably decreases the recirculation that occurred. Equally, they established that the existence of magnetic field disturbs the shear stresses on the wall. The literature reports a series of works in these areas that for brevity are not described here in detail[3-7].

Ferrofluids are materials with super-paramagnetic characteristics, composed of nanoparticles of 8-15nm in diameter[8], suspended in a continuous phase usually an organic or inorganic liquid. These substances have attracted attention due to their particular rheological response, such as, for example, the increase in viscosity in the presence of a permanent magnetic field[9-10], the changes of this parameter due to the effect of a Rotating Magnetic Field (RMF)[11-13], and the generation of flux in the ferrofluid in response to an external RMF[14-19]. Among the applications that have been given to these particular substances, we can highlight the sealing of electronic devices that involve rotating axes[20], applications in micro-electro-mechanical systems[21], heat transfer applications[22], biomedical applications, specifically in controlled drug release processes, in treatments against cancer based on hyperthermia[23], applications in Nuclear Magnetic Resonance (NMR)[24], to mention just a few.

On the other hand, with the objective of describing the behaviour of ferrofluids flow under the effect of a RMF several hypotheses have been proposed, among which the Internal Angular Momentum Diffusion Theory[25] (TDMAI) stands out. It attributes the flow generation to the magnetic nanoparticles rotation, which produces a diffusion of the Internal Angular Momentum (IAM). It in turn generates the rotation of the continuous phase. Additionally, the outset of the flow is also occasioned for the curvature in the fluid-air interface[14]. This hypothesis establishes that the flow of the ferrofluid is generated by tangential magnetic forces that act on these points. In the work reported[15], for a cylindrical geometry, they measured experimental velocity profiles inside a ferrofluid and in the presence of a RMF; using the technique called *Ultrasound Velocity Profile (UVP). These measurements confirmed the existence of a ferrofluid flow, not only on the interfacial surface, but also at points far from the free interface of the fluid. These data showed azimuth velocity profiles with the features of a rigid body movement, co-rotating with the RMF in the internal part of the ferrofluid, in qualitative agreement with TDMAI predictions*[25]. In contrast, the flow direction on the surface of the ferrofluid in contact with air is opposite to the direction of the RMF, as it is established in the work[26]. In the same way, the measurements reported up to that date allowed us to propose that in the flow generation operate two mechanisms of different nature: 1. superficial tangential forces, for the fluid near the ferrofluid-air interface, and 2. volumetric effects, for fluid areas away from the interface. These measurements suggest that the flow fields obtained on the surface are inadequate to validate flow theories, which only apply at points away from it, such as TDMAI, proposed[9-15].

Taking into account the above[27] proposed the description of the flow from the use of a boundary condition of forces, with slippage in the linear moment, and coupled with a slip boundary condition for the internal angular momentum. For this purpose, they implemented the TDMAI for a sample of ferrofluid, contained in an infinitely long rectangular channel in the axial direction, under the effect of a rotating magnetic field (CMR) of low amplitude and frequency. Subsequently, the literature reports similar studies but implemented the proposed magnetization equation Shliomis (Sh-72) and the one proposed by Martsenyuk, Raikher and Shliomis (MRSh-74) in order to compare the results28. These works used a rectangular geometry with a one-dimensional domain, finding, in this way, the profiles according to the vertical coordinate, that is, $\mathbf{v} = \mathrm{v}_z(x)\mathbf{i}_z$ and $\omega = \omega_y(x) i_y$ [27-28].However, although the previous results are the first reported, which assumes a joint effect between volumetric and tangential efforts, do not allow the validation of these, since they are not obtained for a physically achievable geometry. For this reason, in this article the TDMAI is implemented in a square cross section with bidimensional domain, in order to describe the flow fields in all the points of the cross section of the square channel, i.e., $\mathbf{v} = \mathrm{v}_z(x, y)\mathbf{i}_z$ and $\omega = \omega_x(x,y) i_x + \omega_y(x,y) i_y$, which will allow to take into account the presence of the side walls of the duct in the velocity profiles. Consequently, in this paper we present the implementation of the TDMAI, to describe the velocity profiles of ferrofluids under the influence of CMR of high amplitude and frequency, in two-dimensional (square) domain geometry, considering the joint effect of the stresses tangential in the interface and the volumetric efforts in the internal part of the ferrofluid.

This document is organized as follows: after this brief introduction, the hydrodynamic and magnetic equations appear which constitute the central component of the phenomenon math model we are analyzing. Subsequently, the implementation of the numerical methodology to solve the partial differential equation system is shown. This methodology is validated with the analytical solutions, simulating magnetic fields of low amplitude and frequency. Once this validation stage has been carried out, the flow profiles for magnetic fields of high intensity and frequency are generated, with the analysis of results and trends found.

2. Materials and Methods

2.1 System of Hydrodynamic Equations

The continuity equation, the linear momentum balance equation and the internal angular momentum equation, which form the system of hydrodynamic equations, valid for any magnetic field amplitude and any value of the phenomenological coefficient «spin viscosity($\eta' \neq 0$), appear below[29-30] :

$$\tilde{\nabla}.\tilde{v} = 0 \tag{1}$$

$$Re_v \frac{D\tilde{v}}{Dt} = \frac{\zeta}{\tilde{\Omega}\eta}\tilde{M}\cdot\tilde{\nabla}\tilde{H} - \tilde{\nabla}\tilde{p} + \frac{2\zeta}{\eta}\tilde{\nabla}\times\tilde{\omega} + \frac{\eta_e}{\eta}\tilde{\nabla}^2\tilde{v} \tag{2}$$

$$Re_\omega \frac{D\tilde{\omega}}{Dt} = \frac{\zeta}{\tilde{\Omega}\eta}\left(\tilde{M}\times\tilde{H}\right) + 2\tilde{\nabla}\times\tilde{v} - 4\tilde{\omega} + \frac{4\eta}{\eta e}\left(\frac{1}{ve^2+K^2}\right)\tilde{\nabla}\left(\tilde{\nabla}\times\tilde{\omega}\right) + \frac{4\eta}{\eta_e}\tilde{\nabla}^2\tilde{\omega} \tag{3}$$

where $\kappa = \left(\frac{4\eta\zeta R_0^2}{\eta'\eta_e}\right)^{\frac{1}{2}}$, and it is a variable that, even though it has no specific physical meaning, is related to the coefficient of shear viscosity of spin velocity or "spin viscosity η"".

Alternatively, $ve = \left(\frac{4\eta\zeta R_0^2}{\lambda'\eta_e}\right)^{\frac{1}{2}}$, is related to the volumetric coefficient of spin viscosity λ'. Finally, $Re_v = \frac{\rho R_0^2}{\eta}\left(\frac{\mu_0\chi_i K^2 \dot{U}_f}{\zeta}\right)$ and $Re_\omega = \frac{\rho l}{\zeta}\left(\frac{\mu_0\chi_i K^2 \dot{U}_f}{\zeta}\right)$, represent the Reynolds number of translational and spin, respectively. In order to differentiate the variables dimensions, the symbol was included˜, on top of these. The scales of length and time were implemented in the magnetic problem, obtaining equations without dimensions of order one, which were previously reported[29]. Now, to perform the steady-state analysis, an approximation based on the Reynolds number is required, and according to Deen[31], it must be fulfilled that,

$$Re_v \frac{D\tilde{v}}{Dt} = 0, \quad Re_\omega \frac{D\tilde{\omega}}{Dt} = 0. \tag{4}$$

2.2 System of Magnetic Equations

This system is composed of the magnetization equation (Sh-72 or MRSh-74), the Langevin equation and the Maxwell equations.

$$\tilde{\Omega}\frac{\partial\tilde{M}}{\partial t} + \tilde{\Omega}\varepsilon\tilde{v}\cdot\tilde{\nabla}\tilde{M} = \tilde{\Omega}\varepsilon\tilde{\omega}\times\tilde{M} - \tilde{M} + \frac{\mathbf{M_{eq}}}{\chi K}, \tag{5}$$

$$\tilde{\Omega}\frac{\partial\tilde{M}}{\partial t} + \tilde{\Omega}\varepsilon\tilde{\omega}\times\tilde{M} + \frac{\tilde{H}\left(\tilde{H}\bullet\tilde{H}\right)}{\left|\tilde{H}\right|^2}\left(\frac{1}{B_\perp} - \frac{1}{B_\parallel}\right) + \frac{3\tilde{H}\varphi\left(\tilde{H}_x\bullet\tilde{H}_z\right)}{B_\parallel} - + \frac{\tilde{M}}{B_\perp}, \tag{6}$$

$$\varphi\left(\tilde{H}_x\bullet\tilde{H}_z\right) = \frac{\coth(\alpha)}{\alpha} - \frac{1}{\alpha^2} = \frac{\coth\left(\sqrt{\frac{3}{2}\varepsilon\left(\tilde{H}_x^2+\tilde{H}_z^2\right)}\right)}{\sqrt{\frac{3}{2}\varepsilon\left(\tilde{H}_x^2+\tilde{H}_z^2\right)}} - \frac{2}{3\varepsilon\left(\tilde{H}_x^2+\tilde{H}_z^2\right)}, \tag{7}$$

$$\tilde{\nabla}\times\tilde{H} = 0, \tag{8}$$

$$\tilde{\nabla}\cdot\left(\chi\tilde{M} + \tilde{H}\right) = 0. \tag{9}$$

where $\varepsilon = \frac{\mu_0\chi K^2\tau}{\zeta} = \frac{2}{3}\alpha^2$, is called *the perturbation parameter. Similarly, the dimensionless constants of the parallel and perpendicular relaxation times are,*

$$B_\parallel = \frac{\tau_\parallel}{\tau_B} = \frac{d\ln L(\alpha)}{d\ln(\alpha)}, \quad B_\perp = \frac{\tau_\perp}{\tau_B} = \frac{2L(\alpha)}{\alpha - L(\alpha)}, \tag{10}$$

And finally, the Langevin parameter, , is defined as:

$$\alpha = \sqrt{\frac{3}{2}\varepsilon\left|\tilde{H}\right|^2} = \sqrt{\frac{3}{2}\varepsilon\left(\tilde{H}_x^2+\tilde{H}_z^2\right)}.$$

3. Results and Analysis

Next, we present the main simulation results of the ferrofluid flow in a square geometry of flat and parallel plates whose domain is two-dimensional. Figure 1 illustrates the physical situation where the magnetic field is generated by axial field strength H_z and a cross-sectional field density B_x.

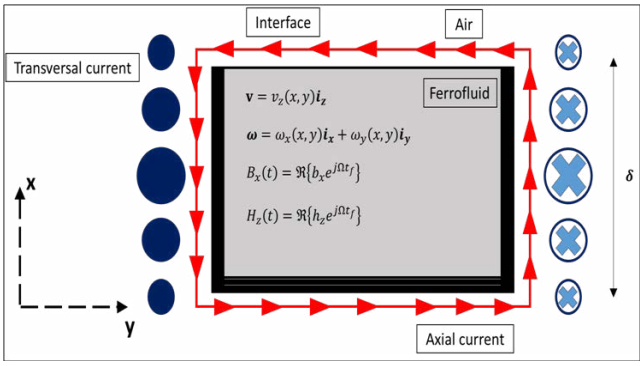

Figure 1. Channel plan of square cross section for the illustrative problem of flow.

3.1 Solution for High Intensity Magnetic Fields

For the case of magnetic fields of high intensity, the internal angular momentum balance equation, including Eq. (4) is:

$$\frac{1}{\tilde{\Omega}}\left(\tilde{M}\times\tilde{H}\right)+2\tilde{\nabla}\times\tilde{v}-4\tilde{\omega}+\frac{4\eta}{\eta_e}\left(\frac{1}{ve^2+\kappa^2}\right)\tilde{\nabla}\left(\tilde{\nabla}\cdot\tilde{\omega}\right)+\frac{4\eta}{\eta_e\kappa^2}\tilde{\nabla}^2\tilde{\omega}=0. \quad (11)$$

Now, with the coordinates in which the internal angular momentum is presented (coordinates x and y), their corresponding scalar equations are deduced as shown:

$$2\frac{\partial\tilde{v}_z}{\partial\tilde{y}}-4\tilde{\omega}+\frac{4\eta}{\eta_e}\left(\frac{1}{ve^2+K^2}\right)\left(\frac{\partial^2\tilde{\omega}_x}{\partial\tilde{x}^2}+\frac{\partial^2\tilde{\omega}_y}{\partial\tilde{y}\partial\tilde{x}}\right)+\frac{4\eta}{\eta_eK^2}\left(\frac{\partial^2\tilde{\omega}_x}{\partial\tilde{x}^2}+\frac{\partial^2\tilde{\omega}_x}{\partial\tilde{y}^2}\right)=0 \quad (12)$$

$$\frac{\langle\tilde{l}_y\rangle_{\tilde{t}}}{\tilde{\Omega}}-2\frac{\partial\tilde{v}_z}{\partial\tilde{x}}-4\tilde{\omega}_y+\frac{4\eta}{\eta_e}\left(\frac{1}{ve^2+K^2}\right)\left(\frac{\partial^2\tilde{\omega}_x}{\partial\tilde{y}\partial\tilde{x}}+\frac{\partial^2\tilde{\omega}_y}{\partial\tilde{y}^2}\right)+\frac{4\eta}{\eta_eK^2}\left(\frac{\partial^2\tilde{\omega}_y}{\partial\tilde{x}^2}+\frac{\partial^2\tilde{\omega}_y}{\partial\tilde{y}^2}\right) \quad (13)$$

In eq. (12) and (13) it can be observed that, unlike the cases studied previously by other authors, cross-related derivatives are presented associated to the horizontal and vertical coordinates of the physical system.

3.2 Methodology of Numerical Solution

In order to illustrate the numerical methodology for the solution to the ferrohydrodynamic system, the flow diagram of Figure 2 is presented.

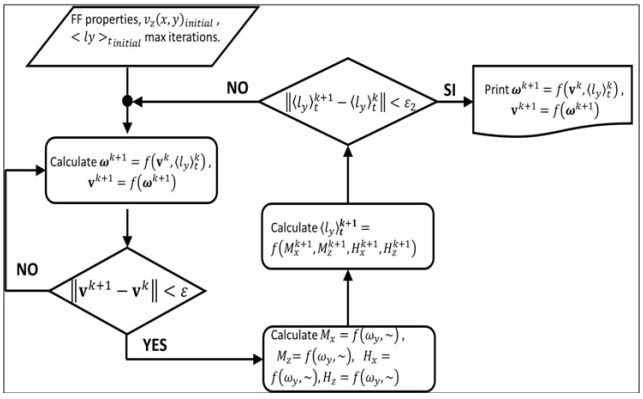

Figure 2. Methodology Flow diagram of the numerical algorithm, ferrohydrodynamic model.

The methodology is described through the following steps:

1. Enter: a. The ferrofluid characteristics, b. The geometry of the container and the physical properties of the system, such as: viscosity of shear η, viscosity of the carrier liquid η_0; initial magnetic susceptibility χ; volumetric fraction ϕ, relaxation time τ (assuming that the nonmagnetic particles with just Brownian type motion, τ_B); the permeability of space μ_0, the magnetic field strength H, the viscosity of vortex ζ, the dimensions of the study system δ, number of system nodes (both geometric and temporal); the initial average torque values at each point of the geometry; and the maximum number of iterations of the algorithm.
2. From the average torque calculated in the previous iteration (in the case of the first iteration, the initial average torque value supplied by the user is assumed), the translational and rotational velocity profiles are calculated, taking into account $\tilde{v}_z = f\left(\tilde{x},\ \tilde{\omega}_y\right)$ that and $\tilde{\omega}_y = f\left(\tilde{x},\tilde{v}_z\right)$.
3. If the velocities do not reach convergence, go back to step 2. Otherwise, it is set to, $\tilde{v}_z\left(\tilde{x}\right)$ and $\tilde{\omega}_y\left(\tilde{x}\right)$, as the velocity profiles corresponding to the average torque value of the iteration and, in this way, the solution of the magnetic problem is continued, in order to obtain the values of, $\tilde{M}_x\left(\tilde{x}\right)$, $\tilde{M}_z\left(\tilde{x}\right)$ $\tilde{H}_x\left(\tilde{x}\right)$ and $\tilde{H}_z\left(\tilde{x}\right)$.
4. The instantaneous torque calculation for each spatial and temporal node of the system under study is carried out. Additionally, the average torque calculation is made for each point of the geometry.
5. If the average torque does not reach convergence, $\geq 1\%$ go back to step 2. Otherwise, it is set $\tilde{v}_z\left(\tilde{x}\right)$ and $\tilde{\omega}_y\left(\tilde{x}\right)$ as the resulting velocity profiles.

3.3 Validation of Algorithm I

A direct way to evaluate the performance of numerical solution algorithms is to obtain the same analytical solutions, when simulating for low intensity fields, where the analytical solutions have physical validity. Starting from the data in Table 1, we proceed to compute the velocity profiles, assuming that $\alpha \ll 1$, and a value of $\eta' = 0$, since for values of $\eta' \neq 0$, there is no analytical solution available so far.

In Figure 3, the curves shown correspond to the profile of $\tilde{v}_z\left(\tilde{x},\tilde{y}\right)$ at half the height of the channel, that is

$\tilde{x} = 0.5$; this is $\tilde{v}_z(0.5; \tilde{y})$. Figure 3, FFT is the analytical solution through the Finite Fourier Transform method and MRSh is the numerical solution of the system implementing the average value of the instantaneous torque obtained by means of the algorithm.

Table 1. Characterization of ferrofluids

Ferrofluido	WBF-1	WGBF-1	GBF-2
$\rho\left(\frac{kg}{m^3}\right)$	1.03	1.26	1.29
$\eta(m)Pas$	1.03	76.1	109
$\eta_0(m)Pas$	1.02	81.2	995
$\mu_0 M_s(mT)$	1.14	2.01	4.02
$\phi(\%)$	0.213	0.376	0.753
χ	0.106	0.200	0.301
$\tau(s)$	1.67×10^{-5}	2.45×10^{-3}	1.84×10^{-3}

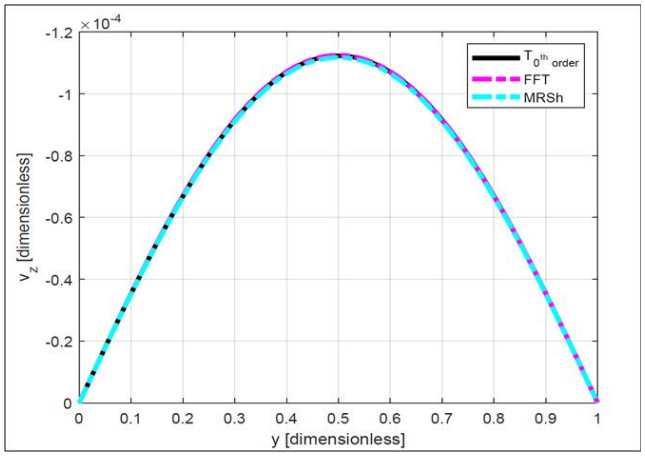

Figure 3. Validation of numerical solutions, of models at low and high fields, with analytical solution.

3.4 Validation of Algorithm II

A second way of validating the results is proposed. For this, numerical simulations are carried out for values of the aspect ratio "a". This parameter in the case of two linear dimensions of an object is called aspect ratio, for example: $\frac{length}{height}$, $\frac{width}{length}$ among others. For this particular case study, the aspect ratio will be defined as the quotient between the width and the height of the channel, that is: $a = \frac{width}{height} = \frac{W}{H}$. It would be expected that, just as the aspect ratio tends to infinity $(a \to \infty)$,

$$\tilde{v}_z(\tilde{x}, \tilde{y})|_{a\to\infty} = \tilde{v}_z(\tilde{x}). \tag{14}$$

As shown in Figures 3&4, there is a match between the numerical and analytical solutions, for this reason, this algorithm will be implemented for the prediction of velocity profiles of ferrofluids contained in a square section channel, under the effect of magnetic fields of high amplitude and frequency, α≫1, where the analytical solutions have no physical validity.

In Figure 4, 2DMS represents the numerical solution of the two-dimensional system (implementing the numerical algorithm for high intensity fields). 1DMS is the analytical solution of the one-dimensional system proposed in the literature (Figures 5&6).

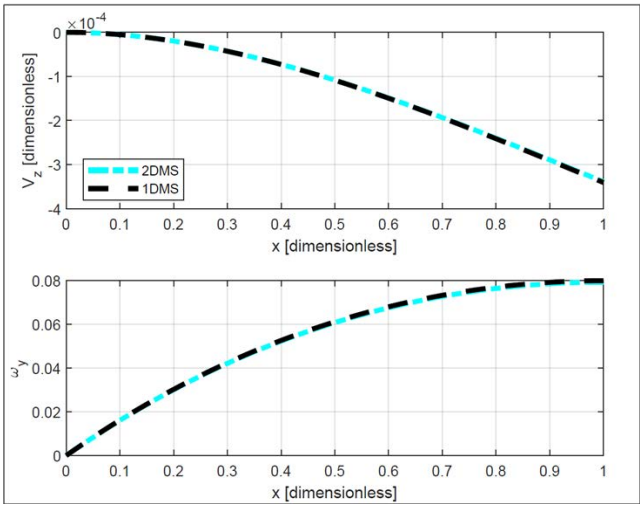

Figure 4. Numerical algorithm validation for $\eta' \neq 0$. Axial linear velocity profiles in $\tilde{y} = 0.5$ [dimensionless].

3.5 Velocity Profiles for $\acute{a} \gg 1$

Next, the results for a magnetic field density of 11, 3 [mT], which is the highest field density reported. In32 for the ferrofluid sample WBF-1, in a cylindrical geometry. This, due to the lack of experimental data, for a square geometry of flat and parallel plates, with which a comparison can be made with the simulation results. Additionally, in Figures 7, 8 and 9 the linear and angular velocity surfaces are presented, along the two-dimensional domain.

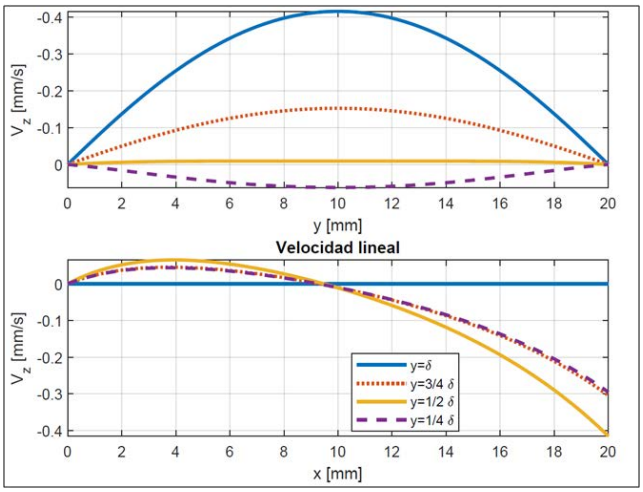

Figure 5. Linear velocity profiles as a function of the horizontal and vertical coordinate for WBF-1.

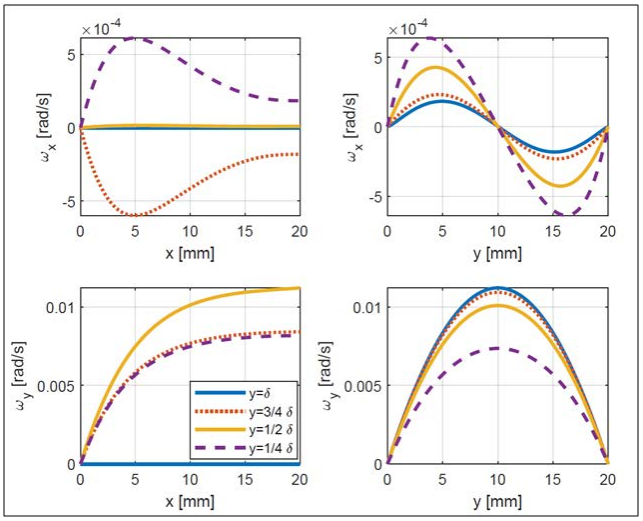

Figure 6. Angular velocity profiles as a function of the horizontal and vertical coordinate for WBF-1.

In Figure 7 a backflow can be seen in the region near the lower wall of the channel (values of x≤5 [mm] approximately), as well as, it can be observed, as in the velocity profiles reported by other authors, that velocities of greater magnitude occur in the points that are part of the ferrofluid-air interface. For its part, in Figure 8&9 it can be observed that the angular velocity ω_y s two orders of magnitude higher than ω_x. Therefore, it could be said that, when taking into account the horizontal coordinate in the analysis, the greater prevalence of the rotation of the particles, as in the results where only the vertical coordinate was taken into account. It is represented in the horizontal component of the angular velocity vector, i.e. ω_y.The former is related to the assumption made initially, where it was defined v_z *(x,y)* s the only component of the translational velocity.Likewise, it can be seen on the surface of angular velocity for ω_x an antisymmetric characteristic, with the axis in y=10 [mm], which represents a counter rotation in the magnetic nanoparticle spin, absent behavior in the surfaces of ω_y.

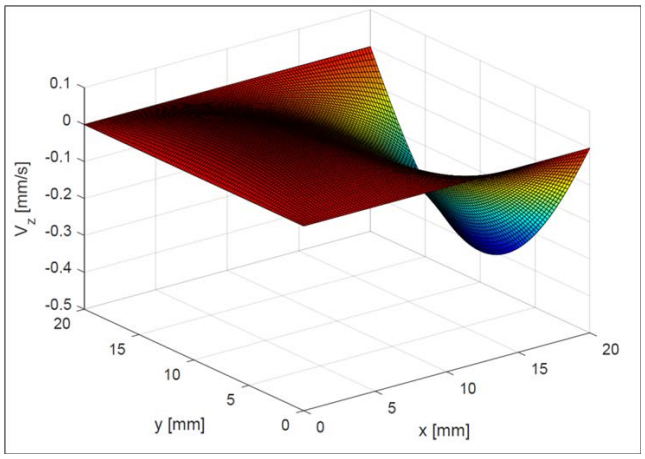

Figure 7. Linear velocity surface v_z depending on the horizontal and vertical coordinate for WBF-1.

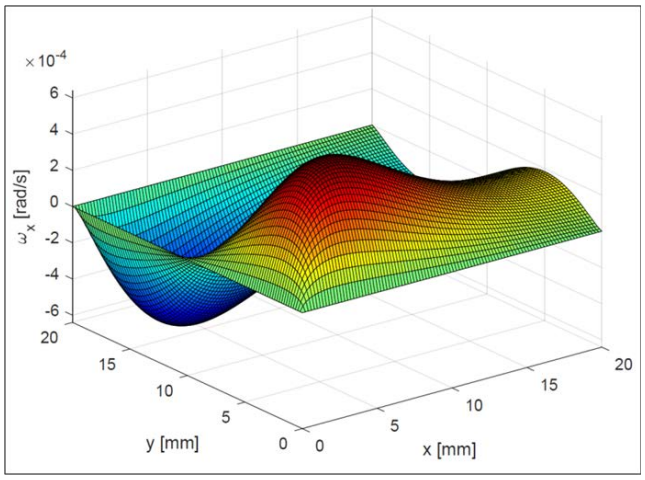

Figure 8. Angular velocity surface ω_x depending on the horizontal and vertical coordinate for WBF-1.

In order to compare the results of the velocity profiles with experimental data reported[32], we obtained from simulation those values for amplitude and frequency magnetic field changes. The sample was WBF-1. The profiles reported in Figure 10 correspond to v_z (x,10 mm), for a channel of flat and parallel plates, whose aspect ratio is one (a=1).As in the experimental results.

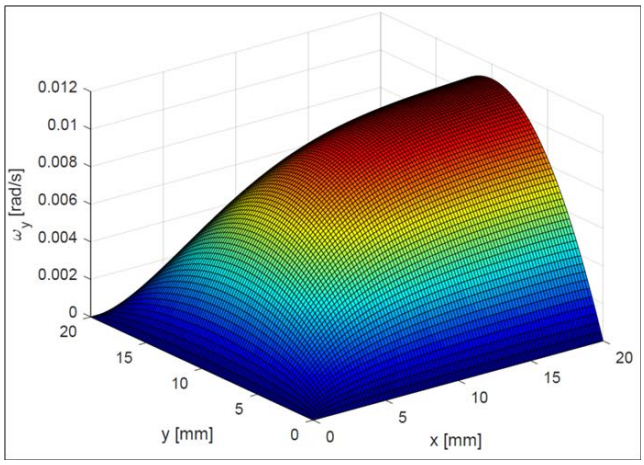

Figure 9. Angular velocity surface ω_y depending on the horizontal and vertical coordinate for WBF-1.

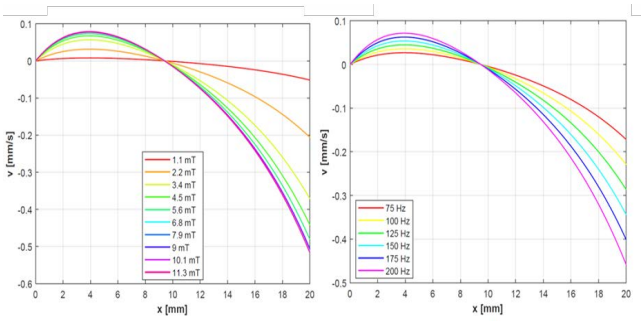

Figure 10. Average velocity profile v_{zi} in the square channel. Left: f=150 [Hz] . Right: B=5,62 [mT].

In[32], despite working with different geometries, you can notice saturation in the magnitude of the velocity, from an approximate value of 7,9 [mT]. According to the results of Figure10, it could be suggested that the saturation phenomenon of the velocity profiles may be more related to the ferrofluid characteristics, than to the geometry of the container in which it is located. Likewise, it can be observed that, for the simulation values implemented, the saturation phenomenon occur when the amplitude value increases, but not the magnetic field frequency. This figure shows the effect of different magnetic field densities (for a constant frequency of 150 [Hz]), and for different frequencies (for a constant magnetic field density of 5,62 [mT]). The profiles are based on the vertical coordinate *X*, for a constant horizontal co-ordinate of y=10 [mm]. For this reason, it is necessary to take into account the operation point in each of the simulation carried out (Figure 11). The extreme values of amplitude and frequency of the magnetic field must be in the curve of constant frequency, α=1,81 and Ω_τ=0,016 (saturation zone), while for the constant magnetic field curve, α=0,90 and Ω_τ=0,021 (zone of non-saturation). Finally, in order to study the effects of increasing the density and the frequency of the magnetic field in the translational velocity, the solution algorithm was operated, with the objective of obtaining the maximum value of translational velocity for a density range of magnetic field between 1-100 [mT]. This according to the field measurements reported in the literature, which is equivalent to a range of the Langevin parameter, $\alpha=[10^{-1}\text{-}10^{1}]$, approximately. The results are presented in Figure 11, in which an increase in the maximum translational velocity is observed, as the magnetic field increases, for a value of the Langevin parameter from 10^{-1} to 10^{0}, approximately. For values of $\alpha \geq 10^{0}$ the saturation phenomenon is presented, from which, when the applied magnetic field intensity increases, the velocity does not show considerable increases. These results cannot be compared with that reported[33-34], due to the lack of knowledge of the characteristics of the ferrofluids used in these experiments, since they were not reported by the authors. On the other hand, the results obtained with the simulations in the bidimensional domain system, with the existence of a ferrofluid-air interface, are in qualitative and quantitative agreement with the data reported[28], with a one-dimensional domain without ferrofluid-air interface. This suggests that, as analyzed with the cylindrical geometry, the saturation phenomenon is more related to the intrinsic thermophysical properties of the ferrofluid, than to the characteristics of the container itself. In this figure, the curve on the left was obtained for the constant frequency f=150 Hz, while the curve on the right for a density B=5,62 [mT].

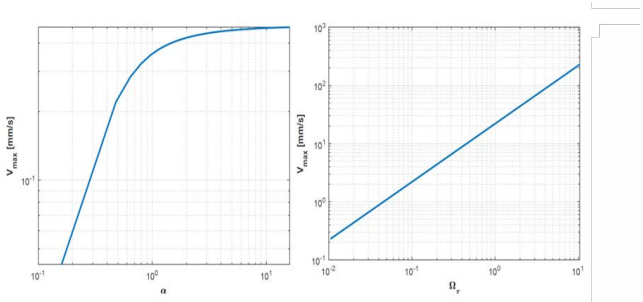

Figure 11. Effect of α and Ω_τ in the maximum values of velocity, v_z, in WBF-1.

4. Conclusions

In this article the combined effect of volumetric and superficial stresses in the flow of ferromagnetic fluids, generated by a RMF, in geometry of flat and parallel plates

of axial length Z infinite was analyzed. In the same way, the TDMAI was implemented to predict the profiles and surfaces of translational velocity and rotation, $\tilde{v}_z\left(\tilde{x},\tilde{y}\right)$, $\tilde{\omega}_x\left(\tilde{x},\tilde{y}\right)$ and $\tilde{\omega}_y\left(\tilde{x},\tilde{y}\right)$ for samples of moving ferrofluids in square geometry ducts.Additionally, the equation MRSh-74 was implemented, within the set of ferrohydrodynamic equations of the TDMAI, in order to predict the velocity profiles, under the effect of high intensity rotating magnetic fields. It should be considered that the profiles of translational velocity and rotation, resulting from the simulations carried out for this article, are valid only for $\lambda' \gg \frac{4\eta\zeta R_o^2}{\eta_e}$. The previous assumption was required to obtain the solution to the system of ferrohydrodynamic equations, Eq. (2) and (3), due to the lack of reported experimental measurements of the volume viscosity coefficient of "spin viscosity", λ', both for the sample of ferrofluid WBF-1 and for other samples of ferrofluids.

5. Acknowledgment

The authors gratefully thank the Universidad Industrial de Santander and Colciencias for the financial support to Cristian Jiménez.

6. References

1. Sharifi A, Motlagh SY, Badfar H. Ferro hydro dynamic analysis of heat transfer and biomagnetic fluid flow in channel under the effect of two inclined permanent magnets, Journal of Magnetism and Magnetic Materials. 2019; 472:115–22. https://doi.org/10.1016/j.jmmm.2018.10.029.
2. Mousavi SM, Darzi AAR, Ali Akbari O, Toghraie D, Marzban A. Numerical study of biomagnetic fluid flow in a duct with a constriction affected by a magnetic field, Journal of Magnetism and Magnetic Materials. 2019; 473:42–50. https://doi.org/10.1016/j.jmmm.2018.10.043.
3. Khokhryakova C, Kostarev K, Shmyrova A. Deformation of ferrofluid floating drop under the action of magnetic field as method of interface tension measurement, Experimental Thermal and Fluid Science. 2019; 101:186–92. https://doi.org/10.1016/j.expthermflusci.2018.10.014.
4. Singh C, Das AK, Das PK. Levitation of non-magnetizable droplet inside ferrofluid, Journal of Fluid Mechanics. 2018; 857:398–448. https://doi.org/10.1017/jfm.2018.733.
5. Gontijo R. Heat transfer increase for a laminar pipe flow of a magnetic fluid subjected to constant heat flux: An initial theoretical approach, Mechanics Research Communications. 2018; 91:27–32. https://doi.org/10.1016/j.mechrescom.2018.05.005.
6. Sharifi A, Yekani Motlagh S, Badfar H. Investigation of the effects of two parallel wires' non-uniform magnetic field on heat and biomagnetic fluid flow in an aneurysm, International Journal Fluid Dynamics. 2018; 32(4-5):248–59. https://doi.org/10.1080/10618562.2018.1490413.
7. Kamis YE, Atalik K. Thermomagnetic effects on the stability of Taylor-Couette flow of a ferrofluid in the presence of azimuthal magnetic field, Journal of Magnetism and Magnetic Materials. 2018; 454:196–206. https://doi.org/10.1016/j.jmmm.2018.01.077.
8. Rosensweig RE. Ferrohydrodynamics. Courier Corporation; 1997. p. 1–344.
9. Shliomis M. Effective viscosity of magnetic suspensions, Soviet Journal of Experimental and Theoretical Physics. 1972; 34(6):1291–94.
10. McTague JP. Magnetoviscosity of magnetic colloids, The Journal of Chemical Physics. 1969; 51(1):133–36. https://doi.org/10.1063/1.1671697.
11. Krekhov AP, Shliomis MI, Kamiyama S. Ferrofluid pipe flow in an oscillating magnetic field, Physics of Fluids (1994-present). 2005; 17(3):33–105.
12. Rinaldi C, Gutman F, He X, Rosenthal AD, Zahn M. Torque measurements on ferrofluid cylinders in rotating magnetic fields, Journal of Magnetism and Magnetic Materials. 2005; 289:307–10. https://doi.org/10.1016/j.jmmm.2004.11.087.
13. Shliomis MI, Morozov KI. Negative viscosity of ferrofluid under alternating magnetic field, Physics of Fluids (1994-present). 1994; 6(8):2855–61.
14. Rosensweig R, Popplewell J, Johnston R. Magnetic fluid motion in rotating field, Journal of Magnetism and Magnetic Materials. 1990; 85(1-3):171–80. https://doi.org/10.1016/0304-8853(90)90046-S.
15. Chaves A, Rinaldi C, Elborai S, He X, Zahn M. Bulk flow in ferrofluids in a uniform rotating magnetic field, Physical Review Letters. 2006; 96(19):194–501. https://doi.org/10.1103/PhysRevLett.96.194501. PMid: 16803104.
16. Moskowitz R, Rosensweig R. Nonmechanical torque-driven flow of a ferromagnetic fluid by an electromagnetic field, Applied Physics Letters. 1967; 11(10):301–03. https://doi.org/10.1063/1.1754952.
17. Chaves A, Torres-Diaz I, Rinaldi C. Flow of ferrofluid in an annular gap in a rotating magnetic field, Physics of Fluids. 2010; 22(9):92–102. https://doi.org/10.1063/1.3483598.
18. Chaves A, Gutman F, Rinaldi C. Torque and bulk flow of ferrofluid in an annular gap subjected to a rotating magnetic field, Transactions of the ASME. 2006; 129(4):412–22.

19. Torres-Díaz I, Rinaldi C. Ferrofluid flow in the annular gap of a multipole rotating magnetic field, Physics of Fluids. 2011; 23(8):82–101. https://doi.org/10.1063/1.3611027.
20. Raj K, Moskowitz B, Casciari R. Advances in ferrofluid technology, Journal of Magnetism and Magnetic Materials. 1995; 149(1-2):174–80. https://doi.org/10.1016/0304-8853(95)00365-7.
21. Jain V, Pant R, Kumar V. Applications of ferrofluids in micro electro mechanical systems (mems) and micropumps, Magnetohydrodynamics. 2008; 44(4):417–24.
22. Bozhko A, Putin G. Magnetic action on convection and heat transfer in ferrofluid, Indian Journal of Engineering and Materials Sciences. 2004; 11(4):309–14. https://www.researchgate.net/publication/228570976_Magnetic_action_on_convection_and_heat_transfer_in_ferrofluid.
23. Medeiros S, Santos A, Fessi H, Elaissari A. Stimuli-responsive magnetic particles for biomedical applications, International Journal of Pharmaceutics. 2011; 403(1-2):139–61. https://doi.org/10.1016/j.ijpharm.2010.10.011. PMid: 20951779.
24. Bautista M, Bomati-Miguel O, Zhao X, Morales M, Gonzalez-Carre-o T, de Alejo RP. Comparative study of ferrofluids based on dextran-coated iron oxide and metal nanoparticles for contrast agents in magnetic resonance imaging, Nanotechnology. 2004; 15(4):154–61. https://doi.org/10.1088/0957-4484/15/4/008.
25. Zaitsev V, Shliomis M. Entrainment of ferromagnetic suspension by a rotating field, Journal of Applied Mechanics and Technical Physics. 1969; 10(5):696–700. https://doi.org/10.1007/BF00907424.
26. Popplewell J, Rosensweig R, Johnston R. Magnetic field induced rotations in ferrofluids, IEEE Transactions on Magnetics. 1990; 26(5):1852–54. https://doi.org/10.1109/20.104546.
27. Chaves A, Rinaldi C. Interfacial stress balances in structured continua and free surface flows in ferrofluids, Physics of Fluids. 2014; 26(4):42–101. https://doi.org/10.1063/1.4869856.
28. Chaves-Guerrero A, Pe-a-Cruz VA, Rinaldi C, Fuentes-Díaz D. Spin-up flow in non-small magnetic fields: Numerical evaluation of the predictions of the common magnetization relaxation equations, Physics of Fluids. 2017; 29(7):73–102. https://doi.org/10.1063/1.4993471.
29. Chaves A, Zahn M, Rinaldi C. Spin-up flow of ferrofluids: Asymptotic theory and experimental measurements, Physics of Fluids. 2008; 20(5):53–102. https://doi.org/10.1063/1.2907221.
30. Jiménez-Leiva C. Evaluación del efecto de la ecuación de magnetización de Martsenyuk, Raikher y Shliomissobre las predicciones de flujo de la teoría de momento angular interno. Universidad Industrial de Santander; 2018. p. 1–20.
31. Deen WM. Analysis of Transport Phenomena, Topics in Chemical Engineering. Oxford University Press; 2011. p. 1–688.
32. Torres-Diaz I, Cortes A, Cedeno-Mattei Y, Perales-Perez O, Rinaldi C. Flows and torques in Brownian ferrofluids subjected to rotating uniform magnetic fields in a cylindrical and annular geometry, Physics of Fluids. 2014; 26(1):120–204. https://doi.org/10.1063/1.4863201.
33. Krauß R, Reimann B, Richter R, Rehberg I, Liu M. Fluid pumped by magnetic stress, Applied Physics Letters. 2005; 86(2):24–102. https://doi.org/10.1063/1.1846956.
34. Krauß R, Liu M, Reimann B, Richter R, Rehberg I. Pumping fluid by magnetic surface stress, New Journal of Physics. 2006; 8(1):1–18. https://doi.org/10.1088/1367-2630/8/1/018.